Detector optimisation for future linear collider

Boruo Xu
of King's College

A dissertation submitted to the University of Cambridge
for the degree of Doctor of Philosophy

Abstract

This is my abstract. To be or not to be.

Declaration

This dissertation is the result of my own work, except where explicit reference is made to the work of others, and has not been submitted for another qualification to this or any other university. This dissertation does not exceed the word limit for the respective Degree Committee.

Boruo Xu

Acknowledgements

Of the many people who deserve thanks, some are particularly prominent, such as my supervisor. . .

Preface

This will be my preface. Where is Wolly?

x

Contents

"Two bags of pork scratchings are worth a bag of gold."
    — Joris the Dutch

Chapter 1

Let's make introduction great again

"Introduction means introdcution"
        — Theresa Trump

Introduction

Chapter 2

Detector

"ILC will be built next year"
　　— Mysterious person

overall

ILC

CLIC

calorimeter

ECal

HCal

Muon chamber

Forward detector

Tracker

Chapter 3

Reconstruction

"How to open a pandora box?"
    — A wise Chinese

3.1 Reconstruction overall

digitisation tracking

3.2 Pandora

Track quality cuts

Iterative track-cluster association

Photon, passage through matter

Muon ID

Fragmentation

3.3 Analysis

3.3.1 Jet algorithm

"exclusive mode", inclusive mode Details

Discussion of why k_t, not durham Longitudinal invariant, k_t, jet algorithm was chosen for the jet clustering. Due to the presence high level of beam induced background at the CLIC, it has been shown that a jet algorithm designed for hadron colliders are more effective than those traditional designed for the electron-positron collider, such as Durham algorithm. []

VLC?

3.3.2 Flavour tagging

3.3.3 MVA

BDT ?likelihood

3.3.4 Jargons

Signal Selection Efficiency Significance

q_l light quark light lepton

Chapter 4

Photon Reconstruction

"Even light can be stopped"
    — Silicon and Tungsten

Chapter 5

Tau Lepton Final State Separation

"MVA: Turn numbers into gold."
    — TMVA

Chapter 6

Double Higgs Bosons Analysis

"Two is better than one"
  — Sir Steve Orange, 1785–1854

6.1 Motivation

Ha there is a higgs.

We found higgs. Higgs is cool. It explains mass.

Why double higgs. Double higgs coulpling is unique to linear collider. It can revel much about the BSM models.

Generator level study has performed. ILC has done this this and that. gHHH in CLIC before

Here we do things differently. First subchannels, then extract both couplings simultaneously.

6.2 Theory

general higgs field

Lagrangian

current constraunt

single higgs coupling measurement done in higgs

Double higgs measurement

The main mechanism for double Higgs production

6.3 Analysis Straggly Overview

Proof-of-principle study was perform at CLIC using CLIC_ILD detector model for $\sqrt{s} = 1.4\,\text{TeV}$ and $3\,\text{TeV}$. Simulated samples, including those containing double higgs production were used. Signal events, events with double higgs production, were selected via a set of carefully designed and complicated methods. g_{HHH} and g_{WWHH} are extracted simultaneously with template fitting with modified couplings samples.

6.4 Monte Carlo Sample Generation

Single channel is defined as $e^-e^+ \rightarrow HH\nu\overline{\nu}$. It is divided into sub-channel $HH \rightarrow b\overline{b}W^+W^-$ and $HH \rightarrow b\overline{b}b\overline{b}$ to allow closer examination and an improvement of signal selection when combined. In particular, I studied $HH \rightarrow b\overline{b}W^+W^-$ sub-channel.

Selected background samples, including processes initiated by photons, are considered in the analysis and listed in Table **??**. These background were expected share similar topologies with the signal process. When describing a multi-quark final state, it is referring to all final states of the same number of quarks, including final states with possible additional neutrinos and or leptons. A multi-quark final state does not include higgs production, unless explicitly stated.

The usual two-quark and four-quark final states were considered. Since the significant presence of beamstrahlung, where photon produced due to the high electric field generated by the colliding beams, processes initiated by photons are also included.

Processes invloving real photons from beamstrahlung (BS) and "quasi-real" photons are generated separately. For the "quasi-real" photon initiated processes, the Equivalent Photon Appproximation (EPA) has been used.

Photon-electron/photon-photon interactions with four-quark final states were considered. Photon-electron interaction with two-quark final state, one Higgs, and one neutrino is considered. Photon-electron interaction with two-quark final state, one Higgs, and one lepton is not considered due to its negligible cross section.

Single higgs productions are not considered because topologies are very different to the single process. Six-quark final states were not considered due to computational limitation.

For processes involving Higgs production explicitly, simulated Higgs mass is 126 GeV. As multi-quark final state background samples could, in principle, contain double higgs production, they are generated with a Higgs mass of 14 TeV. This will produce negligible double higgs production cross section.

All samples are generated with WHIZARD 1.95 [], taking into account the expected CLIC luminosity spectrum. PYTHIA 6.4 [] tuned on LEP data [] is used to describe fragmentation, hadronisation processes, and Higgs decays. TAUOLA [] is used for τ lepton decays.

Simulation

For most background processes, events are simulated when invariant mass of quarks are above 50 GeV. For electron-photon interaction with four quarks and a neutrino final state, events are simulated when invariant mass of quarks are above 120 GeV. These limits are necessary to generate a large amount of background samples in a feasible time, without losing much signal samples.

Finally, the main beam induced background $\gamma\gamma \rightarrow \texttt{hadrons}$ is simulated and overlayed [] to all samples according to the integration time of each subdetector.

6.5 Physics object and event reconstruction

Simulation is performed by MOKKA, interfacing GEANT 4. The reconstruction is done via Marlin in iLCSoft. Separate software package (processor) exists for identification of electrons, muons, taus, and jet reconstruction. New processors have been developed and existing processors have been optimised for a compromise of signal selection and background rejection.

Channel	$\sigma(\sqrt{s} = 1.4\,\text{TeV})$ / fb	$\sigma(\sqrt{s} = 3\,\text{TeV})$ / fb
$e^-e^+ \to HH\nu\overline{\nu}$	0.588	0.149
$e^-e^+ \to q_l q_l H\nu\overline{\nu}$	0.86	1.78
$e^-e^+ \to c\overline{c}H\nu\overline{\nu}$	0.36	1.12
$e^-e^+ \to b\overline{b}H\nu\overline{\nu}$	0.31	1.91
$e^-e^+ \to qqqq$	1245.1	546.5
$e^-e^+ \to qqqq\ell\ell$	62.1	169.3
$e^-e^+ \to qqqq\ell\nu$	110.4	106.6
$e^-e^+ \to qqqq\nu\overline{\nu}$	23.2	71.5
$e^-e^+ \to qq$	4009.5	2948.9
$e^-e^+ \to qq\ell\nu$	4309.7	5561.1
$e^-e^+ \to qq\ell\ell$	2725.8	3319.6
$e^-e^+ \to qq\nu\nu$	787.7	1317.5
$e^-\gamma(BS) \to e^-qqqq$	1160.7	1268.7
$e^+\gamma(BS) \to e^+qqqq$	1156.3	1267.6
$e^-\gamma(EPA) \to e^-qqqq$	287.1	287.9
$e^+\gamma(EPA) \to e^+qqqq$	286.9	287.8
$e^-\gamma(BS) \to \nu qqqq$	136.9	262.5
$e^+\gamma(BS) \to \overline{\nu} qqqq$	136.4	262.3
$e^-\gamma(EPA) \to \nu qqqq$	32.6	54.2
$e^+\gamma(EPA) \to \overline{\nu} qqqq$	32.6	54.2
$e^-\gamma(BS) \to qqH\nu\nu$	15.8	58.6
$e^+\gamma(BS) \to qqH\nu\nu$	15.7	58.5
$e^-\gamma(EPA) \to qqH\nu\nu$	3.39	11.7
$e^+\gamma(EPA) \to qqH\nu\nu$	3.39	11.7
$\gamma(BS)\gamma(BS) \to qqqq$	21406.2	13050.3
$\gamma(BS)\gamma(EPA) \to qqqq$	4018.7	2420.6
$\gamma(EPA)\gamma(BS) \to qqqq$	4034.8	2423.1
$\gamma(EPA)\gamma(EPA) \to qqqq$	753.0	402.7

Table 6.1: List of signal and background samples with the corresponding cross sections at $\sqrt{s} = 3\,\text{TeV}$ and $\sqrt{s} = 1.4\,\text{TeV}$. q can u, d, s, b or t. Unless specified, q, ℓ and ν represent particles and its corresponding anti-particles. γ (BS) represents a real photon from beamstrahlung (BS). γ (EPA) represents a "quasi-real" photon, simulated with the Equivalent Photon Approximation. For processes involving Higgs production explicitly, simulated Higgs mass is 126 GeV. Otherwise, Higgs mass is set to 14 TeV. Simulated W has invariant mass of 80.385 GeV.

For my signal channel, $HH \rightarrow b\bar{b}W^+W^-$, there is no lepton in the final state. Hence a effective lepton identifier would improve the signal identification. Processors are wither developed or optimised with samples at $\sqrt{s} = 1.4\,\text{TeV}$, and checked against samples at $\sqrt{s} = 3\,\text{TeV}$. Because the expected signal significance would be low, the processors are optimised to reject more background at the cost of losing a bit more signals, to increase the signal significance. It was found that the same set of parameters work well under $\sqrt{s}$ = 1.4 TeV and 3 TeV.

6.5.1 Electron and muon identification

IsolatedLeptonFinderProcessor

In Marlin package, IsolatedLeptonFinderProcessor has been used. The optimal parameters ware chosen in collaboration and tested. The particle is identified as an isolated light lepton if it passes a chain of cuts.

A charge track is considered if it has more than $15\,\text{GeV}$ energy. An electron is identified if the energy in the ECal is over 90% of the total calorimetric energy. A muon is identified if the energy in the ECal is between 5% and 25% of the total calorimetric energy. Furthermore, only primary track is selected, which requires the Euclidean distance in the x-y plane, the in z direction, and in the x-y-z three dimensional space of the track starting point to the impact point to be less than $0.02\,\text{mm}$, 0.03mm, and $0.04\,\text{mm}$, respectively. The isolation criteria states that

$$E_{cone}^2 \leqslant 5.7 \times E_l - 50 \tag{6.1}$$

where, E_{cone} is the total energy of PFOs within an opening angle of $\cos^{-1}(0.995)$ of the light lepton, and E_l is the energy of the light lepton.

BonoLeptonFinderProcessor

The IsolatedLeptonFinderProcessor is rather conservative. I developed a new more aggressive light lepton selection processor, BonoLeptonFinderProcessor, that utilises calorimetric information provided by PandoraPFA.

The processor uses two chains of cuts.

First chain uses the particle ID information from PandoraPFA. A electron is identified if it is a "PandoraPFA" electron and the energy in the ECal is over 95% of the total calorimetric energy. A muon is identified if it is a "PandoraPFA" muon. Primary track selection states the Euclidean distance in the x-y-z three dimensional space of the track starting point to the impact point to be less than $0.015\,\mathrm{mm}$, and the PFO energy is more than $10\,\mathrm{GeV}$. The light lepton either satisfy the high p_T requirement of at least $40\,\mathrm{GeV}$, or the isolation criteria,

$$E_l \geqslant 23 \times \sqrt{E_{cone}} + 5 \tag{6.2}$$

where E_{cone} and E_l have the same definition as in the IsolatedLeptonFinderProcessor.

Second chain of cuts is similar to the IsolatedLeptonFinderProcessor. An electron is identified if the energy in the ECal is over 95% of the total calorimetric energy. A muon is identified if the energy in the ECal is between 5% and 20% of the total calorimetric energy. Primary track selection states the Euclidean distance in the x-y-z three dimensional space of the track starting point to the impact point to be less than $0.5\,\mathrm{mm}$, and the PFO energy is more than $10\,\mathrm{GeV}$. The light lepton either satisfy the high p_T requirement of at least $40\,\mathrm{GeV}$, or the isolation criteria,

$$E_l \geqslant 28 \times \sqrt{E_{cone}} + 30 \tag{6.3}$$

where, E_{cone} is the total energy of PFOs within an opening angle of $\cos^{-1}(0.99)$ of the light lepton, and E_l is the energy of the light lepton.

Comparison: IsolatedLeptonFinderProcessor v.s. BonoLeptonFinderProcessor

Two processors share similar criterion for light lepton identification. The main difference is that the BonoLeptonFinderProcessor allows high p_T light lepton to be identified in a potential non-isolated environment, which leads to the more aggressiveness of the BonoLeptonFinderProcessor. The performance of two processors on the signal and selected background samples is shown in table 6.2

6.5.2 Tau identification

TauFinderProcessor

With a decay length of $87\,\mu m$, tau leptons decay before reaching the detector and can only be identified through the reconstruction of their decay products. The leptonic decay of tau can be identified using the two isolated lepton finder processor. Therefore tau identification will focus on the hadronic decay.

TauFinderProcessor, an existing processor Marlin package, has been tuned in collaboration and tested. The a collection of tau decay productions are identified they pass a chain of cuts.

Particles are not considered if p_T is less than $1\,\mathrm{GeV}$ or $|\cos(\theta_Z)|$ is more than $1.1\,\mathrm{rad}$, as they are more likely from beam induced background. A seed is considered if a charged particle has p_T more than $10\,\mathrm{GeV}$. A search cone of opening angle $0.03\,\mathrm{rad}$ is then formed. The search cone is rejected if it has more than 3 charged particles, more than 10 particles or its invariant mass more than $2\,\mathrm{GeV}$. An isolation cone is formed with opening angle between 0.03 and $0.33\,\mathrm{rad}$ of the seed. The seed is rejected if there are more than $3\,\mathrm{GeV}$ in the isolation cone.

BonoTauFinderProcessor

The TauFinderProcessor's performance is decent, but there is room for improvement. I developed a new more aggressive tau lepton selection processor, BonoTauFinderProcessor, that utilises calorimetric information provided by PandoraPFA.

Similar to the previous processor, PFOs with p_T less than $1\,\mathrm{GeV}$ are rejected. A tau seed is defined as a charged particle with p_T at least $5\,\mathrm{GeV}$. The search cone has an opening angle of $\cos^{-1}(0.999)$. Particles are iteratively added to the search cone according to the size of the opening angle to the seed. A temporary search cone is then considered if it has one or three charged particles, and the invariant mass is less than $3\,\mathrm{GeV}$. The search cone needs to satisfy one of isolation criterion.

1. No particle in the large isolation cone, and p_T of search cone at least $10\,\mathrm{GeV}$,

2. One charged particle in the search cone, one particle in the large isolation cone, and r_0 larger than $0.01\,\mathrm{mm}$,

Selection / Efficiency (1.4 TeV)	Signal	$qqqq\ell\nu$
IsolatedLeptonFinderProcessor	99.3%	50.3%
BonoLeptonFinderProcessor	99.1%	39.9%
TauFinderProcessor	97.5%	52.3%
BonoTauFinderProcessor	89.7%	38.5%
ForwardFinderProcessor	98.9%	95.1%
Combined	86.6%	16.8%
Processor / Efficiency (3 TeV)	Signal	$qqqq\ell\nu$
IsolatedLeptonFinderProcessor	99.5%	66.8%
BonoLeptonFinderProcessor	99.0%	52.5%
TauFinderProcessor	97.7%	79.5%
BonoTauFinderProcessor	86.3%	60.3%
ForwardFinderProcessor	95.9%	80.7%
Combined	81.0%	23.3%

Table 6.2: isolated lepton finder processors performance on the signal and selected background samples.

3. Three charged particle in the search cone, one particle in the large isolation cone, p_T of search cone at least 10 GeV, and search cone opening angle less than $\cos^{-1}(0.9995)$,

4. One charged particle in the search cone, no particle in the small isolation cone, r_0 larger than 0.01 mm, and p_T of search cone at least 10 GeV,

5. Three charged particle in the search cone, no particle in the small isolation cone, p_T of search cone at least 10 GeV, and search cone opening angle less than $\cos^{-1}(0.9995)$,

where large and small isolation cone are defined as opening angle of $\cos^{-1}(0.95)$, and $\cos^{-1}(0.99)$ respectively. If there are multiple temporary search cone of a same seed passing the isolation criteria, the cone with smallest opening angle is chosen for output.

Comparison: TauFinderProcessor v.s. BonoTauFinderProcessor

Two processors share similar size of search cone and isolation cone. The BonoTauFinder-Processor has looser cut on minimum p_T and invariant, but stricter isolation criterion. This leads to a more aggressive tau finder. The performance of two processors on the signal and selected background samples is shown in table 6.2

6.5.3 Very forward electron identification

Certain background channels, for example photon-electron interactions, contain electrons in the very forward part of the detector, namely LCal and BCal. These forward calorimeters were not simulated due to computational limitation. Most particle in these detector would be very forward particles from beam induced background. However, previous study has shown [] that high energy electrons can be identified with high efficiency. Due to the lack of tracking in these region, electrons and photons would have the same electromagnetic shower profile, with the given calorimeter resolution. MC photons and electrons are checked if they fall in the LCal or the BCal, and checked against the known detection efficiency.

Beam Calorimeter acceptance is defined as $|\cos(\theta_Z)|$ is between 0.01 and 0.04 rad and length in z direction is between 3181 and 3441 mm. Luminosity Calorimeter acceptance is defined as $|\cos(\theta_Z)|$ is between 0.038 and 0.11 rad and length in z direction is between 2539 and 2714 mm. For $\sqrt{s} = (\text{TeV } 3)$, the BeamCal detection efficiency is provided by a software package []. For $\sqrt{s} = (\text{TeV } 1.4)$, the same software for the BeamCal is used, by scaling the energy of the MC particle by a factor of $\frac{3}{1.4}$. For the LumiCal, the identification efficiency is defined as

$$\varepsilon = \begin{cases} 0, & \text{if } E < 50\,\text{GeV} \\ 0.99 \times \frac{(\text{erf}(E-100)+1)}{2}, & \text{otherwise} \end{cases} \tag{6.4}$$

where E is the energy of the electron or the photon.

The background rejection is significant, shown in table **??** for the signal and selected background.

6.5.4 Other lepton identification processors

Other isolated lepton selection processors available in Marlin package, including IsolatedLeptonTagging and TauJetClustering, have been tested. The results, after some tuning of parameters, were unsatisfactory. They either performed poorly comparing to the processors above, or became redundant after the processors above. Therefore, these processors were not used in this analysis.

Selection / Efficiency (1.4 TeV)	Signal	$e^-\gamma(BS) \to e^-qqqq$
Combined light lepton finder	87.6%	67.5%
ForwardFinderProcessor	98.9%	53.6%
Combined	86.6%	30.8%
Processor / Efficiency (3 TeV)	Signal	$e^-\gamma(BS) \to e^-qqqq$
Combined light lepton finder	84.4%	72.7%
ForwardFinderProcessor	95.9%	55.4%
Combined	81.0%	33.4%

Table 6.3: Very forward electron and photon finder performance on the signal and selected background samples.

6.6 Jet reconstruction

The signal channel, $HH \to b\bar{b}W^+W^- \to b\bar{b}qqqq$, is a four-jet final state. A useful technique for the analysis is to reconstruct the four-jet final state using jet algorithms. This allows discriminative variables to be calculated.

6.6.1 Jet reconstruction optimisation

Longitudinal invariant, k_t, jet algorithm was chosen for the jet clustering. Due to the presence high level of beam induced background at the CLIC, it has been shown that a jet algorithm designed for hadron colliders are more effective than those traditional designed for the electron-positron collider, such as Durham algorithm. []

The free parameters for k_t algorithm is the R parameter, which controls the fatness of the jet. There is also the choice of the PFO collection, which incorporate different level of time and p_T cuts, to reduce beam induce background. Both parameters are optimised for $\sqrt{s} = 1.4\,\text{TeV}$ and $\sqrt{s} = 3\,\text{TeV}$.

The details of jet algorithm can be found in section **??**.

The R parameter of the k_t jet algorithm, and the collection of the PFOs are chosen to give the best invariant mass resolution. When there are a few suitable candidate, analysis were performed in parallel. Decision were made to give the highest signal significance.

k_t jet algorithm was used as part of the FastJet algorithms available in the Marlin package.

The samples containing the signal, $HH \to b\bar{b}W^+W^- \to b\bar{b}qqqq$, was used for the optimisation of the jet reconstruction. The signal events were chosen using MC truth information.

Jet algorithm was run in exclusive mode, where number of jets is chosen to be six.

For the signal, $HH \to b\bar{b}W^+W^- \to b\bar{b}qqqq$, one Higgs decays to two b quarks, resulting in two jets from hadronisation. Similarly the other Higgs decays to two W bosons, where each W boson decays into two quarks. Therefore, the expected number of jets is six.

Jets produced by the k_t jet algorithm are paired up using MC truth information, to the corresponding Higgs and W boson. Four invariant mass distributions are obtained: two Higgs masses, $m_{H_{bb}}$, $m_{H_{WW^*}}$, and two W masses m_W, m_{W^*}. W^* indicates the off-mass-shell W boson, because when a Higgs decays into two W bosons, one W is off the mass shell, as the Higgs mass is less than the sum two W masses.

Three mass distributions are worth comparing for different jet reconstruction, namely, $m_{H_{bb}}$, $m_{H_{WW^*}}$, and m_W. The ideal jet reconstruction should produce the a sharp mass peak around the particle's true mass.

To quantitatively access the mass distribution, a gaussian like fit is performed to extract the position of the peak, and the width of the distribution. The fit has the form:

$$f(m) = Ae^{-\frac{(m-\mu)^2}{g}} \begin{cases} g = 2\sigma_L + \alpha_L(m-\mu), & \text{if } m < \mu \\ g = 2\sigma_R + \alpha_R(m-\mu), & \text{if } m \geqslant \mu \end{cases} \tag{6.5}$$

The fit represents an asymmetrical gaussian function, where m is binned mass distribution, with 50 bins in range $[0, 200]\,\text{GeV}$. The fitted mass peak is denoted by μ. σ_L and σ_R allow asymmetrical width of the distribution. α parameter controls the fit of tails. Inspired by the $t\bar{t}$ analysis [], the use of the α parameter allows the fit in the whole mass range, otherwise only the peak of the distribution should be fitted with a gaussian like function. A is the normalistion factor. An example of the fit of $m_{H_{bb}}$ is shown in figure 6.1.

For $\sqrt{s} = 1.4\,\text{TeV}$, shown in figure 6.2, normal selected PFO with $R = 0.7$ give a good fitted mass for H_{WW^*} and W. The mass is slightly too low for the H_{bb}. figure 6.3 shows the combined relative fitted width for the H_{bb}, H_{WW^*} and W. Normal selected PFO with $R = 0.7$ gives an almost optimal relative width for H_{bb}, while achieving a good balance
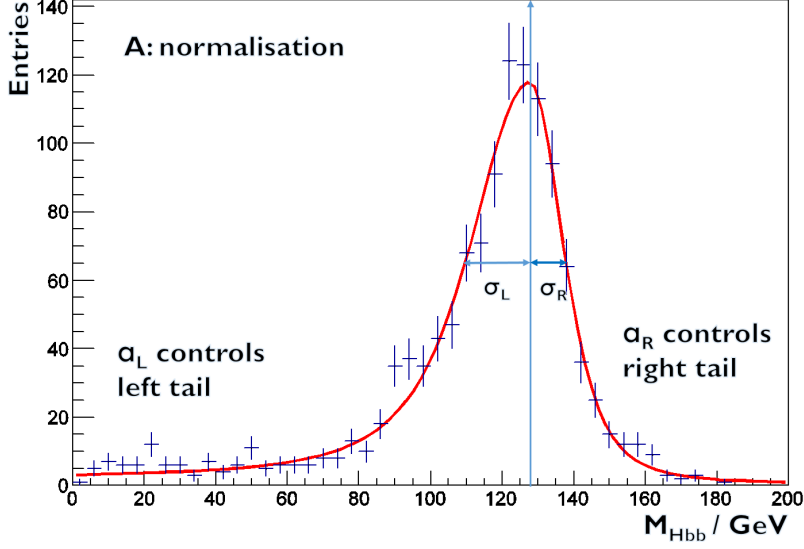
Figure 6.1: A typical example of MC mass fit of $m_{H_{bb}}$ for double higgs analysis. Red line indicates the best fit. Vertical arrow indicates the fitted peak position.

for H_{WW^*} and W. Therefore, normal selected PFO with $R = 0.7$ is chosen to be the optimal jet reconstruction parameters.

For $\sqrt{s} = 3\,\text{TeV}$, the choice is a bit more complicated. Shown in figure 6.4, fitted mass for H_{bb} favours normal selected PFO with $R = 0.8$. Fitted mass for H_{WW^*} favours tight selected PFO with $R = 0.9$. Fitted mass for W favours tight selected PFO with $R = 0.8$. Looking at the combined relative fitted width for the H_{bb}, H_{WW^*} and W, shown in figure 6.5, normal selected PFO gives a larger width than tight selected PFO. Within tight selected PFO, small R values provide a shaper width for H_{WW^*} and H_{bb}, but a broader width for W. Therefore, tight selected PFO with $R = 0.7$ and $R = 1$ are both chosen for parallel analysis.

Later it was shown that tight selected PFO with $R = 0.7$ gives a better signal significance. Therefore the optimal choice of jet reconstruction for $\sqrt{s} = 3\,\text{TeV}$ is tight selected PFO with $R = 0.7$.

The extracted fitted parameters of optimal jet reconstructions are summarised in table 6.4.
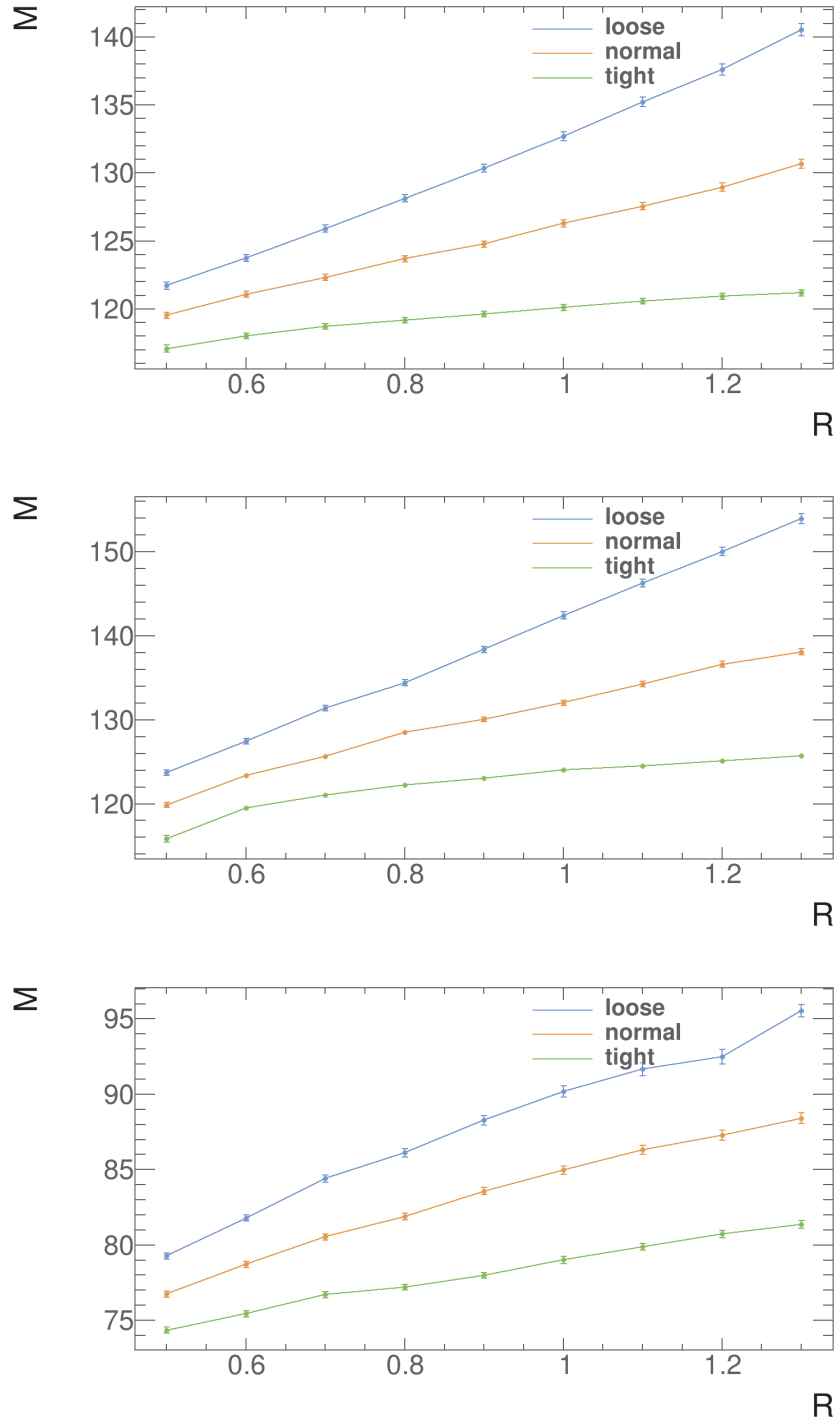
Figure 6.2: Fitted mass and statistical error of H_{bb}, H_{WW^*} and W for $\sqrt{s} = 1.4\,\text{TeV}$, for loose, normal and tight selected PFO against R parameter.
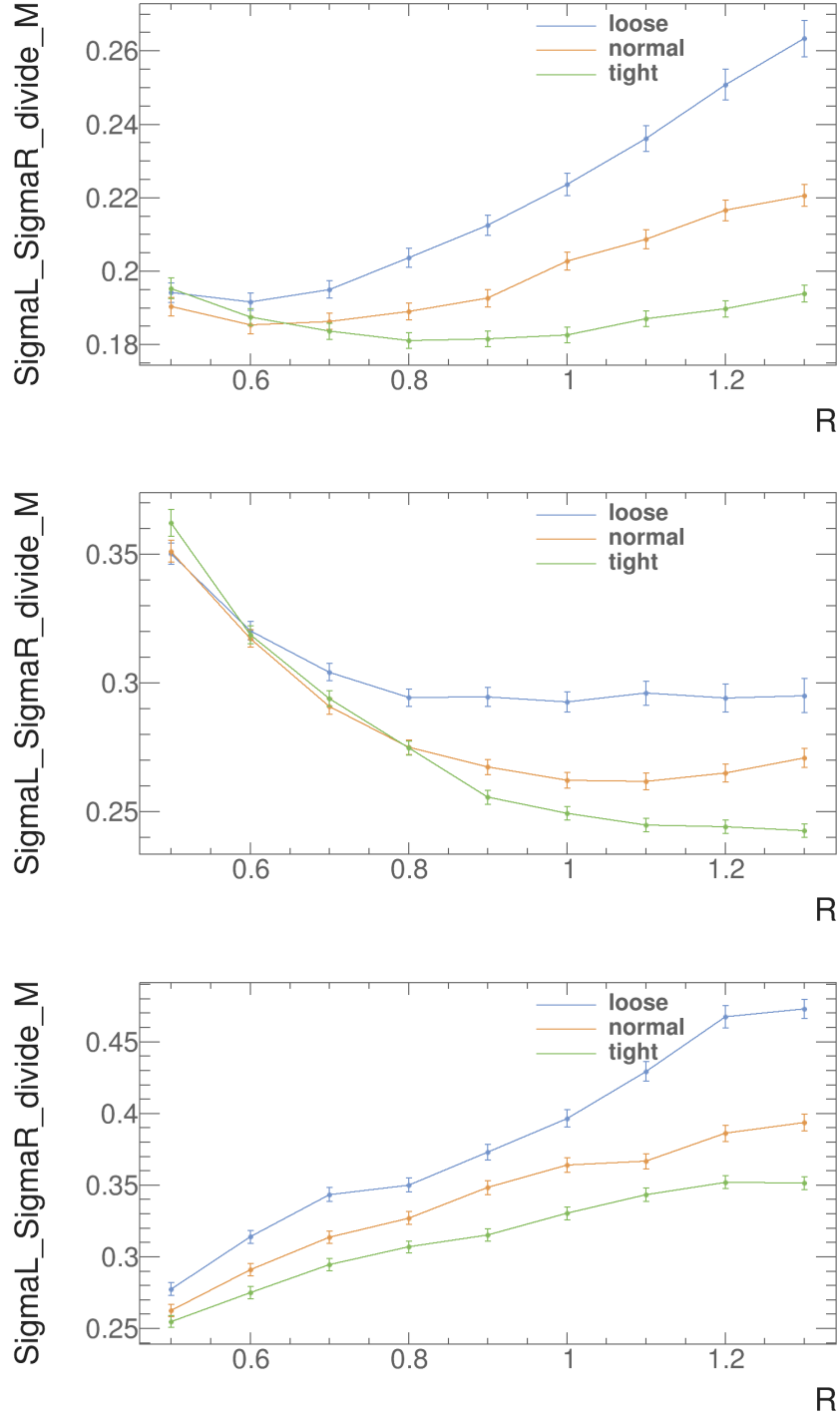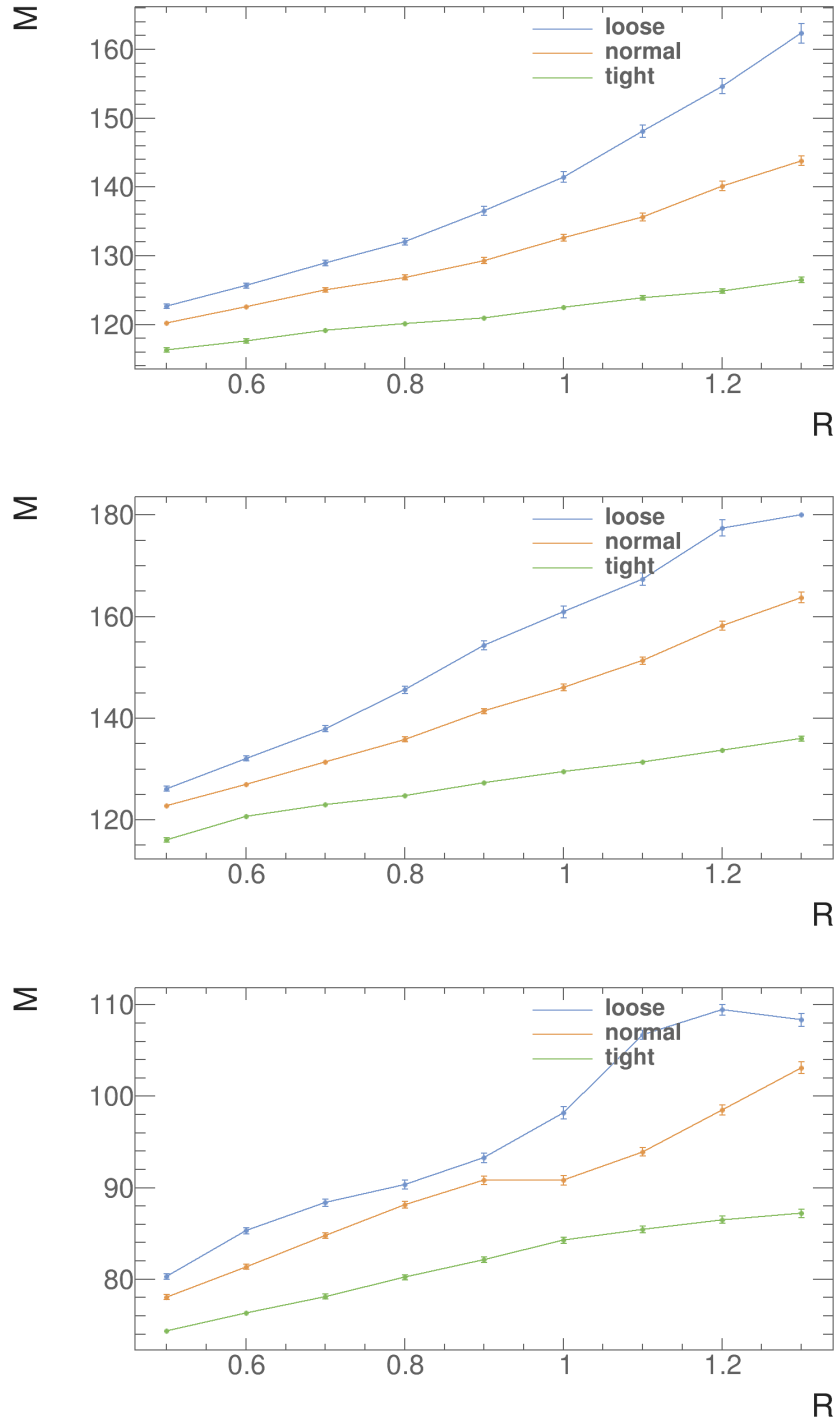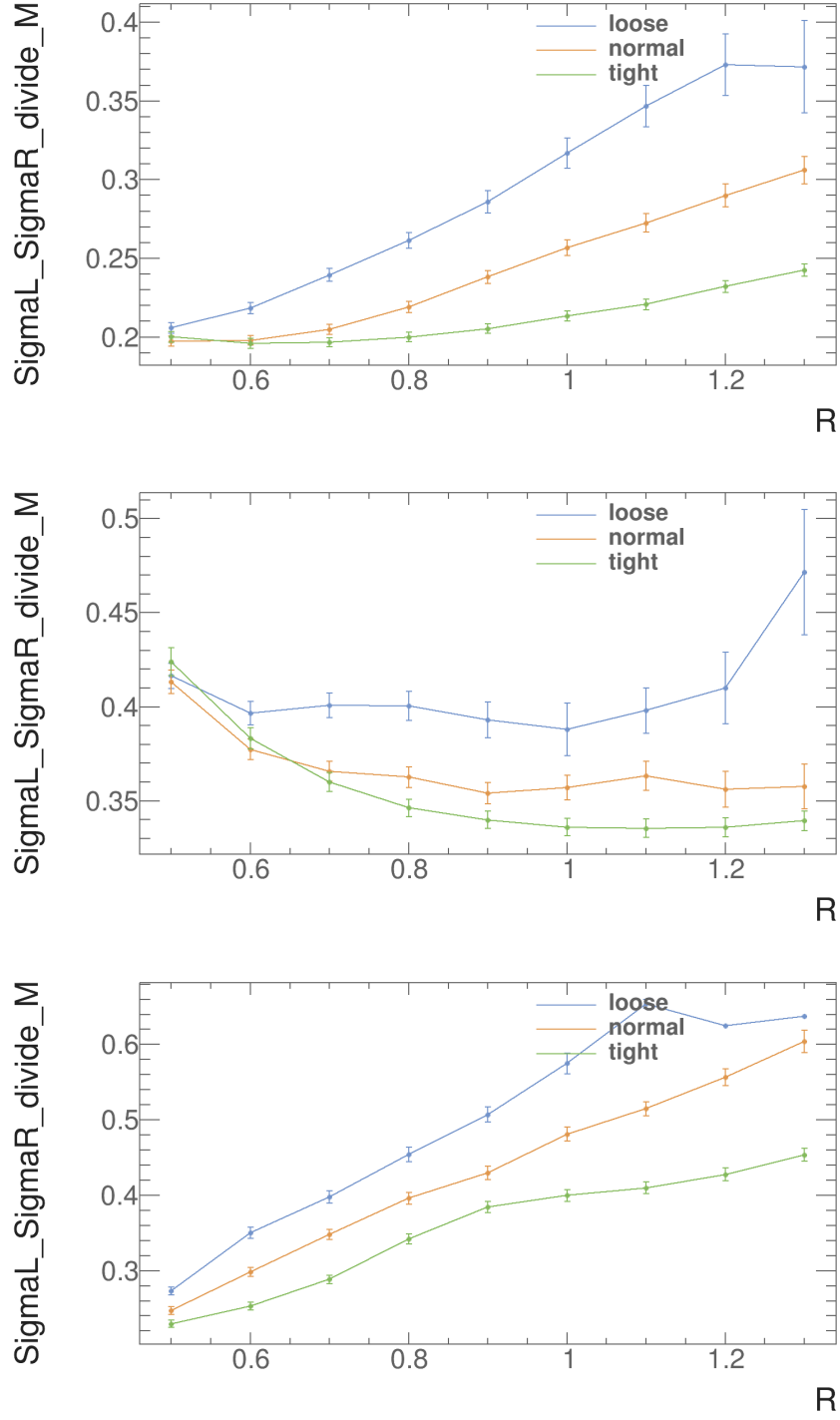
Figure 6.3: Fitted combined width and statistical error of H_{bb}, H_{WW^*} and W for $\sqrt{s} = 1.4\,\mathrm{TeV}$, for loose, normal and tight selected PFO against R parameter.

Figure 6.4: Fitted mass and statistical error of H_{bb}, H_{WW^*} and W for $\sqrt{s} = 3\,\text{TeV}$, for loose, normal and tight selected PFO against R parameter.

Figure 6.5: Fitted combined width and statistical error of H_{bb}, H_{WW^*} and W for $\sqrt{s} = 3\,\text{TeV}$, for loose, normal and tight selected PFO against R parameter.

Jet Parameters	$\sqrt{s} = 1.4\,\mathrm{TeV}$	$\sqrt{s} = \mathrm{S\,TeV}$
$\mu_{H_{bb}}$	$122.3_{\pm 0.2}$	$119.1_{\pm 0.3}$
$\sigma_{L,H_{bb}}$	$15.2_{\pm 0.2}$	$15.0_{\pm 0.3}$
$\sigma_{R,H_{bb}}$	$7.55_{\pm 0.16}$	$8.4_{\pm 0.2}$
$\mu_{H_{WW^*}}$	$125.7_{\pm 0.2}$	$123.0_{\pm 0.3}$
$\sigma_{L,H_{WW^*}}$	$29.4_{\pm 0.3}$	$36.6_{\pm 0.6}$
$\sigma_{R,H_{WW^*}}$	$7.18_{\pm 0.17}$	$7.4_{\pm 0.2}$
μ_W	$80.5_{\pm 0.2}$	$78.1_{\pm 0.3}$
$\sigma_{L,W}$	$16.2_{\pm 0.3}$	$13.1_{\pm 0.4}$
$\sigma_{R,W}$	$9.03_{\pm 0.16}$	$9.5_{\pm 0.2}$

Table 6.4: The extracted fitted parameters of optimal jet reconstructions, normal selected PFO with $R = 0.7$ for $\sqrt{s} = 1.4\,\mathrm{TeV}$ and tight selected PFO with $R = 0.7$ for $\sqrt{s} = 3\,\mathrm{TeV}$.

6.6.2 Jet flavour tagging

Two b-jets out of six jets in final states are identified with flavour tagging processors. The processor calculates a set of discriminatively variables for a jet. After training the MVA, the MVA is applied to jets to produce a likelihood for b-jet and c-jet. For details see section **??**.

The existing LCFIPlus processor in Marlin package is used. The training sample of the flavour tagging processor is $e^-e^+ \rightarrow Z\nu\bar{\nu}$, where Z decays to $q_l\bar{q}_l$, $b\bar{b}$, or $c\bar{c}$ at $\sqrt{s} = 1.4\,\mathrm{TeV}$ and $\sqrt{s} = 3\,\mathrm{TeV}$, because they have similar event topology as the signal, and they have only two jets in the final state.

The selection efficiency of b-jets and c-jets with trainning samples are shown in figure **??**. Flavour tagging performs better at low energy. Because at high energy, particles at more collimated and more difficult to separate.

6.6.3 Jet pairing

The jet pairing was performed by seaking combination of jets that are compatible with signal $HH \rightarrow b\bar{b}W^+W^-$.

(a) $\sqrt{s} = 1.4\,\mathrm{TeV}$ **(b)** $\sqrt{s} = 3\,\mathrm{TeV}$
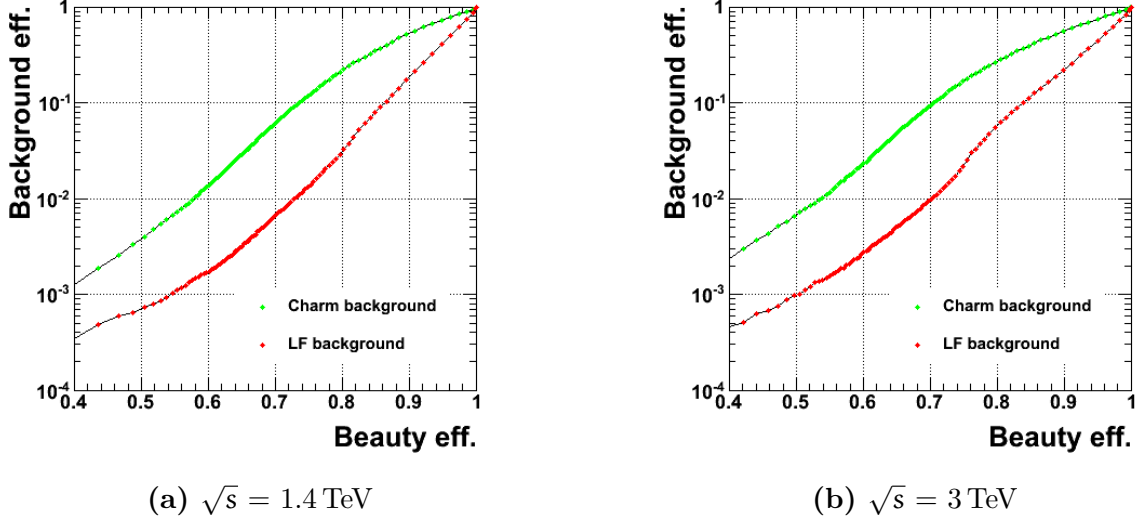
Figure 6.6: Performance of b-jet tagging with trainning samples

The actual pairing is done via a minimisation

$$\chi^2 = \left(\frac{m_{ij} - \mu_{H_{bb}}}{\sigma'_{H_{bb}}}\right)^2 + \left(\frac{m_{klmn} - \mu_{H_{WW^*}}}{\sigma'_{H_{WW^*}}}\right)^2 + \left(\frac{m_{kl} - \mu_{W}}{\sigma'_{W}}\right)^2, \qquad (6.6)$$

where, $\mu_{H_{bb}}$ and $\sigma'_{H_{bb}}$ are the fitted invariant mass, and the fitted width, respectively. Both are obtained in section 6.6.1. $\sigma'_{H_{bb}}$ is $\sigma_{L,H_{bb}}$ when $m_{ij} < m_{H_{bb}}$, and $\sigma_{R,H_{bb}}$ otherwise. Similarly $\mu_{H_{WW^*}}$ and μ_W are fitted mass, and $\sigma'_{H_{WW^*}}$ and σ'_W are fitted invariant mass, and the fitted width, respectively. Out of the six jets from the jet clustering, indicated by subscript i, j, k, l, m, n, two are used for H_{bb}, two for W and four for H_{WW^*}. The fitted parameters used are listed in table 6.4

Colophon

This thesis was made in LaTeX 2_ε using the "hepthesis" class [1].

Bibliography

[1] A. Buckley, The hepthesis LaTeX class.

List of figures

List of tables